PERGAMON

International Journal of Heat and Mass Transfer 43 (2000) 963–980

International Journal of HEAT and MASS TRANSFER

www.elsevier.com/locate/ijhmt

A computational study of transient plane front solidification of alloys in a Bridgman apparatus under microgravity conditions

V. Timchenko [a], P.Y.P. Chen [a], E. Leonardi [a], G. de Vahl Davis [a,*], R. Abbaschian [b]

[a] *School of Mechanical and Manufacturing Engineering, University of New South Wales, Sydney, NSW 2052, Australia*
[b] *Department of Materials Science and Engineering, University of Florida, Gainesville, FL 32611, USA*

Received 17 August 1998; received in revised form 18 May 1999

Abstract

A mathematical model of heat, momentum and solute transfer during directional solidification of binary alloys in a Bridgman furnace has been developed. A fixed grid single domain approach (enthalpy method) is used. The effects of coupling with the phase diagram (a concentration-dependent melting temperature) and of thermal and solutal convection on segregation of solute, shape and position of the solid/liquid interface are investigated. A vorticity–stream function formulation is used for calculation of the velocity fields. The results presented include calculations at 1 and 10 μ*g*, both neglecting and including the dependence of melting temperature on concentration. © 2000 Published by Elsevier Science Ltd. All rights reserved.

Keywords: Crystal growth; Solidification; Microgravity; Bridgman furnace; Computational

1. Introduction

The investigation of solidification processes has great practical importance for crystal growth techniques. The quality of single crystals grown from the melt depends strongly on growth morphology and macro-segregation caused by convection effects in solidified ingots. A low gravity environment is often used for fundamental studies of crystal growth because it produces conditions in which convection is eliminated or at least decreased to a level at which crystal growth is largely controlled by diffusion. Residual accelerations in orbiting space vehicles are of the order of one to several hundred μ*g* (where 1 μ$g = 9.81 \times 10^{-6}$ m s^{-2}). For this reason, much effort has been expended in recent years in performing crystal growth experiments in the microgravity environment of a spacecraft in earth orbit. Such effects as compositional and kinetic supercooling, and the influence of convection on compositional distribution in the melt, have been investigated under microgravity.

The MEPHISTO-4 Program is a joint US–French–Australian research effort directed towards gaining a detailed understanding of the role of buoyancy-driven convection during the directional solidification of faceted materials in a Bridgman apparatus, specifically

* Corresponding author. Tel.: +61 2 9385 4099; fax: +61 2 9663 1222.
E-mail address: g.devahldavis@unsw.edu.au (G. de Vahl Davis).

0017-9310/00/$ - see front matter
PII: S0017-9310(99)00176-3

Nomenclature

B	buoyancy ratio, $((\beta_C C_r)/(\beta_T \Delta T_r)$
c_p	specific heat at constant pressure
C	solute concentration
D	solute diffusivity
f	volume fraction
F	convection flux
g	gravity acceleration
G	imposed temperature gradient
h	enthalpy
H	ampoule height
k	time step
k_p	partition coefficient
L	latent heat
Le	Lewis number, α/D
m	slope of liquidus line
p	iteration number
Pr	Prandtl number, $c_p\mu/\lambda$
q	diffusion flux
R	interface velocity
Ra	Rayleigh number, $\rho g\beta\Delta T_r H^3/\alpha\mu$
S_c	source term
St	Stefan number, $c_p\Delta T_r/L$
t	time
T	temperature
T_m	melting temperature
V	velocity
u	velocity component in x-direction
v	velocity component in y-direction
α	thermal diffusivity
β_C	solutal expansion coefficient
β_T	thermal expansion coefficient
ΔT_r	$T_h - T_c$
Δx	mesh size in x-direction
Δy	mesh size in y-direction
γ	characteristic parameter
γ_c	solute segregation at the interface
λ	thermal conductivity
μ	viscosity
ρ	density
ξ	distance measured from interface
ψ	stream function
ζ	vorticity

Subscripts

ave	average value
c	cold zone
cr	critical
h	hot zone
I	interface
i,j	grid point
l	liquid
min	minimum value
max	maximum value
n	normal direction
r	reference value
s	solid
sens	sensible heat
ϕ	phase
0	initial value

Superscripts

$\sim$	vector
$\wedge$	unit vector
k	time step
p	inner iteration
$'$	dimensionless quantity

an alloy of bismuth with 1 at% tin. It combines ground-based experiments and a series of experiments conducted in a microgravity environment. Part of this program is a numerical modelling of the solidification process.

The MEPHISTO apparatus, shown schematically in Fig. 1, consists of three parallel tubes or ampoules (only one is shown in the figure), each containing the Bi–Sn alloy, around which are placed two 'furnaces', each comprising a pair of heating and cooling jackets. Between each heating and cooling jacket is a nominally adiabatic or insulated zone. One furnace is fixed, and acts to generate a reference state; the other can be moved over the tubes. If it moves in the direction from the cooling to the heating jacket (i.e., to the right in Fig. 1), and if the heating and cooling rates are chosen appropriately, the material will be progressively solidified from left to right.

Many numerical investigations of solidification of alloys in different Bridgman growth configurations have been carried out in recent years. Chang and Brown [1] studied radial segregation induced by natural convection in a vertical Bridgman cavity for dilute alloys. Adornato and Brown [2] considered both dilute and concentrated alloys with convection driven by both temperature and concentration gradients. Alexander et al. [3] investigated the effects of residual acceleration on dopant distribution in Bridgman–Stockbarger crystal growth with different gravity vector orientations. Yao et al. [4] evaluated the effects of various gravity levels on solute segregation for vertical and horizontal Bridgman growth configurations.

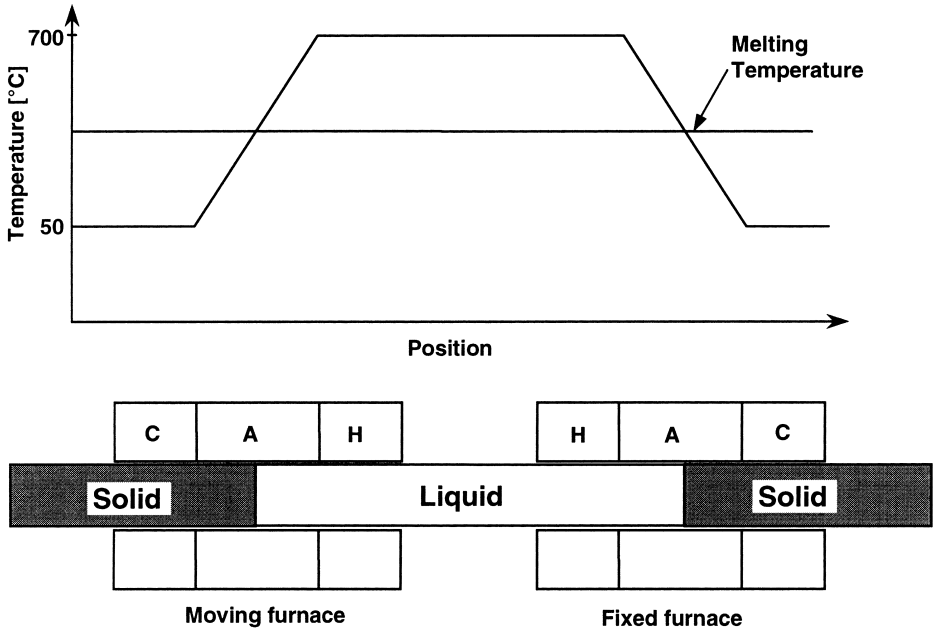

Fig. 1. Schematic diagram of the MEPHISTO apparatus, and the nominal boundary temperature distribution. H and C denote the hot and cold sections of the furnaces; A denotes the adiabatic zone.

In all of these works a pseudo steady-state model was adopted. This is a simplification of the true unsteady solidification process, and neglects transient effects such as changes in the velocity, temperature and concentration with time due to changes in the length of melt caused by translating the ampoule. It was also assumed that the melting temperature at the interface is constant and hence that the rate of solidification is the same as the rate of furnace translation. In reality the melting temperature changes with concentration during the initial transients, thus producing a lagging of the interface movement compared with steady growth. Investigation of solute redistribution during the initial transients becomes crucial for an alloy with a low partition coefficient solidifying at low rates because the steady state is difficult to reach in laboratory experiments.

For modelling transient phase change processes, a fixed grid single domain approach (commonly called the enthalpy method) appears to be more applicable due to its relative simplicity and low computational cost compared with front tracking methods. It has been used successfully for modelling various complicated phase-change systems including dendritic structures [5,6]. Single domain models reduce the general multiphase system to a single continuum medium and permit the solution of the conservation equations to be obtained in the entire domain including the solid, liquid and what is known as the mushy zone (if any). The boundary conditions applied at the solid–liquid interface in multi-domain methods are replaced by source terms in the energy, momentum and (for alloys) solute conservation equations [7]. A number of mathematical models for binary liquid–solid phase change problems using a fixed grid have been developed [8], most of them for alloys which solidify over a temperature-range.

In the Bridgman configuration with low growth speeds and high thermal gradients in the adiabatic zone, the interface stays sharp and phase change has to be treated as isothermal, i.e., there is no mushy zone or transition region between the solid and the liquid. Implementation of the enthalpy method for modelling the isothermal phase change of alloys becomes quite a challenging problem because of the additional difficulties associated with the discontinuity of solute concentration at the interface and sharp gradients of concentration at the interface induced by the low value of partition coefficient. These are the conditions, which apply in MEPHISTO.

2. Mathematical model

We consider a Bridgman furnace in which a moving temperature profile consisting of a cold zone (T_c), a nominally adiabatic zone and a hot zone (T_h) is imposed on the boundary of the ampoule. This boundary temperature profile is translated with a constant pulling velocity as a result of the furnace movement

causing the solid/liquid interface to move along the ampoule. The material in the ampoule is thus divided into two sub-regions: solid and liquid.

Although the ampoule is three-dimensional, a two-dimensional model is used. This simplification is valid because, under the microgravity conditions being considered, convection is very weak and the solidification process remains largely diffusion-controlled and to some extent even one-dimensional. Newtonian and laminar flow is assumed in the liquid phase, and the Boussinesq approximation has been used, in which the liquid density is assumed to be constant except in the buoyancy term of the equation of motion.

The governing time dependant equations describing mass, momentum, heat and solute transport in the vorticity–stream function formulation are:

$$\rho\left(\frac{\partial\zeta}{\partial t}+\nabla\cdot\left(\tilde{V}\zeta\right)\right)=\nabla\rho\times\hat{g}|g|+\mu\nabla^2\zeta \tag{1}$$

$$\nabla^2\psi=-\zeta \tag{2}$$

$$\rho c_{\mathrm{p}}\left(\frac{\partial T}{\partial t}+\nabla\cdot\left(\tilde{V}T\right)\right)=\lambda\nabla^2T \tag{3}$$

$$\frac{\partial C}{\partial t}+\nabla\cdot\left(\tilde{V}C\right)=D\nabla^2C \tag{4}$$

where ρ,μ, c_{p}, λ and D are, respectively, the density, viscosity, specific heat and thermal conductivity of the alloy and the diffusivity of the solute; ζ, ψ, T, $\tilde{V}$ and C are respectively the vorticity, stream function, temperature, velocity vector and solute concentration; g is the magnitude of the gravitational acceleration, and $\hat{g}$ is the unit vector in the direction of gravity. The density in the buoyancy term of Eq. (1) is assumed to be a linear function of temperature and solute concentration:

$$\rho=\rho_{\mathrm{r}}\left[1-\beta_T(T-T_{\mathrm{r}})+\beta_C(C-C_{\mathrm{r}})\right] \tag{5}$$

where β_T and β_C are the (assumed constant) thermal and solutal expansion coefficients, defined by

$$\beta_T=-\frac{1}{\rho_{\mathrm{r}}}\frac{\partial\rho}{\partial T} \tag{6}$$

and

$$\beta_C=\frac{1}{\rho_{\mathrm{r}}}\frac{\partial\rho}{\partial C} \tag{7}$$

ρ_{r}, T_{r} and C_{r} are reference values of density, temperature and concentration.

Latent heat evolution during phase change is incorporated in the energy equation by introducing a source term for enthalpy. For each phase ϕ, enthalpy is defined as

$$h=\int_0^T c_{\mathrm{p}_\phi}\,\mathrm{d}T+f_{\mathrm{l}}L, \tag{8}$$

where L is the latent heat and f_{l} is a local liquid volume fraction.

With the assumption that specific heat c_ϕ is constant in each phase, Eq. (8) can be written as

$$h=c_{\mathrm{p}_\phi}T+f_{\mathrm{l}}L=h_{\mathrm{sens}}+f_{\mathrm{l}}L, \tag{9}$$

in which h_{sens} is the sensible heat. Using the apparent heat capacity method [9], an effective specific heat can be defined by

$$C^*(T)=\frac{\partial h}{\partial T}=c_{\mathrm{p}_\phi}+L\frac{\partial f_{\mathrm{l}}}{\partial T}. \tag{10}$$

Using Eq. (10), the energy equation (3) can be written as

$$\rho\left[C^*(T)\frac{\partial T}{\partial t}+c_{\mathrm{p}_\phi}\nabla\cdot\left(\tilde{V}T\right)\right]=\lambda\nabla^2T. \tag{11}$$

To solve Eq. (11), an effective heat capacity coefficient $\partial f_{\mathrm{l}}/\partial T$ has to be calculated. We define

$$\frac{\partial f_{\mathrm{l}}}{\partial T}=\frac{\partial f_{\mathrm{l}}/\partial n}{\partial T/\partial n}=\frac{(f_{\mathrm{l}})_nT_n}{T_n^2}=\frac{(f_{\mathrm{l}})_xT_x+(f_{\mathrm{l}})_yT_y}{T_x^2+T_y^2} \tag{12}$$

where subscripts n (denoting the normal direction), x and y denote differentiation.

As the temperature distribution on the boundary and hence the solid/liquid interface moves, the solid sub-region of the computational domain increases in length. In the solid, the vorticity, stream function and velocities are set to zero. In the liquid, they are calculated from the stream function defined as

$$\tilde{V}=\nabla\times\tilde{\psi}. \tag{13}$$

2.1. Solute transport with phase change

The most difficult problem in modelling solute transport during solidification is associated with the discontinuity of solute concentration at the interface. Additional difficulties occur due to the presence of a thin solute boundary layer in the liquid in which large solute gradients develop, induced by the low partition coefficient. The basic assumptions in the analysis are:

- Thermodynamic equilibrium exists at the solid–liquid interface: $T_{\mathrm{m}}=T_{\mathrm{s}}=T_{\mathrm{l}}$ and $C_{\mathrm{s}}=k_{\mathrm{p}}C_{\mathrm{l}}$, where k_{p} is the partition coefficient.
- Solute diffusion in the solid phase is negligible.
- The solid phase is stationary and a distinct separation of the phases exists at the interface.

- The densities and thermal conductivities of the liquid and solid phases are constant and equal.

A source term accounting for the release of solute into the liquid during solidification is derived by considering the average concentration in an arbitrary control volume which is undergoing phase change [7]. This control volume can be treated as partially solidified with an average concentration defined as

$$C = f_s C_s + f_l C_l \tag{14}$$

where $f_s = 1 - f_l$ is the local solid volume fraction. Since diffusion in the solid is neglected, C_s at any position in the interior of the solid is not a function of time and $\partial C_s/\partial t = 0$. Noting that $C_s = k_p C_l$ at the interface, Eq. (14) may then be differentiated to yield

$$\frac{\partial C}{\partial t} = -\frac{\partial f_s}{\partial t}(1 - k_p)C_l + (1 - f_s)\frac{\partial C_l}{\partial t}. \tag{15}$$

The first term on right-hand side of Eq. (15) can be interpreted as the change in the concentration determined by the mass flux at the solidification front which is moving with velocity $R = (\partial f_s/\partial t)\Delta x$, releasing solute into the liquid due to differences in the solid and liquid concentration at the interface. Here Δx is the size of control volume in the direction of solidification. The second term is associated with the fact that this release occurs in the liquid fraction of the partially solidified control volume. Eq. (15) is used in place of the first term on the left-hand side of Eq. (4). In the other terms, C is replaced by C_l since Eq. (4) applies only to the liquid region. This leads to

$$\frac{\partial C_l}{\partial t} + \nabla \cdot (\tilde{V} C_l) = D\nabla^2 C_l + S_c \tag{16}$$

where

$$S_c = \frac{\partial f_s}{\partial t}(1 - k_p)C_l + f_s \frac{\partial C_l}{\partial t}. \tag{17}$$

Eqs. (16) and (17) apply to liquid concentration only and hence bypass the concentration discontinuity at the interface.

During the initial transients of solidification, the melting temperature varies with time due to changes in the concentration of the solute. With the assumption that phase change takes place under local thermodynamic equilibrium, the temperature at the interface — the melting temperature $T_m(C)$ — can be expressed as

$$T_m(C) = T_{m0} + mC_I \tag{18}$$

where T_{m0} is the melting temperature of pure solvent, C_I is the interface solute concentration, m is slope of the liquidus, assumed to be constant and obtained from the phase diagram for the particular alloy.

2.2. Calculation of liquid fraction

For isothermal phase change, the liquid fraction is determined by the melting temperature T_m:

$$\text{for } T > T_m \quad f_l = 1$$

$$\text{for } T < T_m \quad f_l = 0. \tag{19}$$

T_m in turn is determined by the cell average solute concentration in the liquid portion of each cell containing the interface. The liquid fraction undergoes a step change when the interface crosses a grid line, which can cause serious numerical instabilities. To overcome this problem, a control volume was defined around each grid point, in which the liquid fraction could be estimated. Phase change is considered to take place over one control volume, in which Eq. (19) is replaced by a linear approximation:

$$\text{for } T_{i,j} > T_m + \Delta T \quad f_l = 1$$

$$\text{for } T_m - \Delta T \le T_{i,j} \le T_m + \Delta T \quad f_l = (T_{i,j} - T_m + \Delta T)/2\Delta T \tag{20}$$

$$\text{for } T_{i,j} < T_m - \Delta T \quad f_l = 0.$$

Here $2\Delta T$ is a temperature interval chosen so that the time taken for the computational cell to change temperature by $2\Delta T$ due to the boundary temperature profile translation is approximately the same as the time necessary for the cell to change phase completely.

In directional solidification, the direction of interface movement is known. This fact can be used with advantage to evaluate the liquid fraction. If the cell boundary temperatures in the direction of crystal growth are $T_{i-1/2,j}$ and $T_{i+1/2,j}$, respectively, and the melting point is T_m, the liquid fraction f_l is given by

$$f_l = \frac{T_{i+1/2,j} - T_m}{T_{i+1/2,j} - T_{i-1/2,j}}. \tag{21}$$

Based on the calculated values at each mesh point of liquid fraction the computational domain is subdivided into sub-regions of solid and liquid phases in the following manner. If the liquid fraction in a particular (i,j) point is calculated to be less than or equal to 0.5, the corresponding cell is defined as being 'solid' for the purpose of computing the flow: the velocities, vorticity and stream function there are set to zero. If the liquid fraction is greater than 0.5, the cell is defined as being 'liquid', and the flow calculations are as normal. The interface position is determined using the value of the liquid fraction. To account for the evolution of latent heat and release of solute during solidification, the

cells where the liquid fraction is between zero and one are treated as partially solidified cells.

2.3. Non-dimensional equations

Using H (the height of the ampoule), H^2/α (where α is the thermal diffusivity) and α/H as scale factors for length, time and velocity, respectively, defining non-dimensional temperature and concentration by

$$T' = \frac{T - T_c}{\Delta T_r} \quad \text{and} \quad C' = \frac{C}{C_r} \tag{22}$$

where $\Delta T_r = T_h - T_c$, and using primes to denote non-dimensional quantities, we obtain Eqs. (1), (2), (11) and (16) in the following forms:

$$\frac{\partial \zeta'}{\partial t'} + \nabla \cdot (\tilde{V}' \zeta') = Ra\, Pr(\nabla T' \times \hat{g} - B \nabla C' \times \hat{g}) + Pr \nabla^2 \zeta' \tag{23}$$

$$\nabla^2 \psi' = -\zeta', \tag{24}$$

$$\frac{\partial T'}{\partial t'}\left(1 + \frac{1}{St}\frac{\partial f_l}{\partial T'}\right) + \nabla \cdot (\tilde{V}' T') = \nabla^2 T', \tag{25}$$

$$\frac{\partial C_l'}{\partial t'} + \nabla \cdot \left(\tilde{V}' C_l'\right) = \frac{1}{Le} \nabla^2 C_l' + S_C. \tag{26}$$

3. Solution method

An algorithm entitled SOLCON,[1] which incorporates the closely coupled solution of the transport equations in the vorticity–stream function formulation, was developed. In this algorithm, a modified alternating direction implicit (ADI) Samarskii–Andreyev scheme [10] is used to solve iteratively the vorticity, stream function, energy and solutal equations at each time step. The modification achieves accurate coupling between the transient equations and the boundary conditions and hence a true transient 'simultaneous' solution of the equations. Since the temperature boundary profile is moving in discrete time steps, obtaining an accurate true transient solution is impossible without having all equations converged at each time step. Apart from that, the use of iterations becomes necessary because of the strong non-linearity of all governing equations. To ensure stability of the computational process, all source terms and non-linear coefficients depending on liquid fraction are linearized based on the value of liquid fraction obtained from the previous iteration.

The vorticity, stream function and energy equations were discretized using central differences and solved by the modified ADI scheme with internal iterations. Interface boundary conditions for vorticity and stream function were applied at those mesh points in the solid sub-region which are adjacent to the liquid. For the calculation of vorticity boundary conditions, the definition of vorticity was used: $\tilde{\zeta} = \nabla \times \tilde{V}$. The boundary condition $\psi = 0$ was used for the stream function.

3.1. Concentration equation

The concentration Eq. (26) required special treatment. It was discretized and solved using the control volume approach. This ensures mass balance during phase change in the partially solidified control volume. Integration of Eq. (26) over a control volume and discretization uniformly in each direction yields

$$\begin{aligned}
&\frac{C'^{\,k}_{i,j} - C'^{\,k-1}_{i,j}}{\Delta t}\Delta x \Delta y + F_{i+1/2,j} - F_{i-1/2,j} + F_{i,j+1/2} - F_{i,j-1/2} \\
&= \frac{1}{Le}\left[\left(D'_{i+1/2,j}\frac{C'_{i+1,j} - C'_{i,j}}{\Delta x} - D'_{i-1/2,j}\frac{C'_{i,j} - C'_{i-1,j}}{\Delta x}\right)\Delta y \right. \\
&\left. + \left(D'_{i,j+1/2}\frac{C'_{i,j+1} - C'_{i,j}}{\Delta y} - D'_{i,j-1/2}\frac{C'_{i,j} - C'_{i,j-1}}{\Delta y}\right)\Delta x\right] + S_C \Delta x \Delta y
\end{aligned} \tag{27}$$

where F is the convection flux integrated over the control volume face:

$$\begin{aligned}
&F_{i+1/2,j} = (u'C')_{i+1/2,j}\Delta y \qquad F_{i-1/2,j} = (u'C')_{i-1/2,j}\Delta y \\
&F_{i,j+1/2} = (v'C')_{i,j+1/2}\Delta x \\
&F_{i,j-1/2} = (v'C')_{i,j-1/2}\Delta x.
\end{aligned} \tag{28}$$

For simplicity we omit the index 'l' showing that the equation is being solved only for liquid concentration C_l. Eq. (27) was solved over the whole computational domain, although for all cells defined as 'solid', the liquid concentration was set to zero.

To resolve the sharp gradients of concentration in the vicinity of interface, a second order upwind scheme

[1] SOLidification and CONvection.

[11] was used to discretize the convection fluxes. This was chosen because it is more stable than central differences, particularly for problems with low diffusion coefficients and hence high Lewis numbers. It is considerably more accurate than first order upwind schemes but more complex since it uses a four-point stencil for calculating the fluxes.

$$(u'C')_{i+1/2,j} = \left(\frac{u'_{i+1/2,j} + |u'_{i+1/2,j}|}{2}\right) \times \left(\frac{3C'_{i,j} - C'_{i-1,j}}{2}\right) + \left(\frac{u'_{i+1/2,j} - |u'_{i+1/2,j}|}{2}\right) \times \left(\frac{3C'_{i+1,j} - C'_{i+2,j}}{2}\right) \quad (29)$$

where $u'_{i+1/2,j}$ is the velocity component on the $(i+1/2, j)$ face of the control volume. Central differences were used for the diffusion terms.

The non-dimensional diffusion coefficients on the faces of the control volume were set to one or zero depending on whether $T_{i+1/2,j}$ is greater than (or equal to) T_m, or is less than T_m.

To account for the interface movement through the partially solidified control volume, the diffusion flux in the direction of solidification, $q'_{i+1/2,j}$, integrated over the control volume face Δy was written as

$$q'_{i+1/2,j} = D'_{i+1/2,j}\frac{C'_{i+1,j} - C'_{i,j}}{\Delta x^*}\Delta y \quad (30)$$

where $\Delta x^* = 0.5(f_l + 1)\Delta x$ is the distance between the centre of the liquid portion of a partially solidified control volume and the centre of the next control volume. Convection and diffusion fluxes in the direction normal to solidification have been integrated over liquid fractions of the control volume faces $f_l\Delta x$.

3.2. Extrapolation procedure for interface concentration

The computed solute concentration can oscillate when the phase change front moves from one cell into the next. The reason is that in a fixed grid finite volume formulation, the computed values of C are cell averaged values. As the interface moves from one cell to the next, C suddenly drops from one value to a lower value. The concentration in the new cell then increases due to progressive solute rejection at the interface, which occurs at a rate faster than diffusion out of the control volume. The problem becomes even more difficult when variations of melting temperature with solute concentration are taken into consideration. The concentration-dependent melting temperature obtained from Eq. (18) will have an unrealistic zigzag shape and hence will not be suitable for the calculation of the liquid fraction and the estimation of interface position. To overcome this problem and to account for the fact that the computed concentration is a cell average value, an exponential extrapolation procedure based on the liquid fraction has been introduced to find the value of the concentration at the solid/liquid interface.

For steady, diffusion-controlled, unidirectional solidification, the solute build-up in front of the interface can be described by an exponential function [12]. We assumed a similar expression at each time step:

$$C(\xi) = C_I e^{-\gamma\xi} \quad (31)$$

where γ is a quantity to be determined and ξ denotes distance in the x-direction measured from the interface.

Let $C_{i,j}$ denote the average concentration in the liquid portion of the (i, j) control volume:

$$\int_0^{f_l\Delta x} C(\xi)\,d\xi = C_{i,j} f_l \Delta x. \quad (32)$$

Then Eqs. (31) and (32) yield

$$C_{i,j} = \frac{\int_0^{f_l\Delta x} C_I e^{-\gamma\xi}\,d\xi}{f_l\Delta x} = \frac{C_I(1 - e^{-\gamma f_l\Delta x})}{\gamma f_l \Delta x}. \quad (33)$$

Using a Taylor series for the exponential function and neglecting third order and higher terms, we obtain

$$C_I = \frac{C_{i,j}}{1 - 0.5\gamma f_l \Delta x}. \quad (34)$$

The parameter γ can be found from the interface condition

$$\left(\frac{\partial C}{\partial x}\right)_I = -\frac{R}{D}(1 - k_p)C_I \quad (35)$$

where R is the growth or interface velocity $(\partial f_s/\partial t)\Delta x$. Differentiation of Eq. (31) together with Eq. (35) gives following expression for γ:

$$\gamma = \frac{R}{D}(1 - k_p). \quad (36)$$

The interface solute concentration C_I calculated from Eq. (34) can be used to couple the temperature and solute fields through Eq. (18) and to calculate the concentration in the solid as it forms. It is a smooth function of time (or position), as will be shown below. The zigzag shape resulting from the use of $T_m(C)$ is eliminated. This extrapolation procedure is useful even when T_m is constant, as it readily enables a smooth

Table 1
Property values and other quantities used in the computations

Property	Symbol	Value
Density	ρ	10,070 kg/m^3
Specific heat	c_p	144.87 J/kg K
Thermal conductivity	λ	12.4 W/m K
Thermal diffusivity	α	8.500×10^{-6} m^2/s
Viscosity	μ	1.85×10^{-3} kg/m s
Diffusion coefficient for Sn in Bi	D	2.7×10^{-9} m^2/s
Thermal expansion coefficient	β_T	1.25×10^{-4} K^{-1}
Solutal expansion coefficient	β_C	-0.305 (kg Sn/kg alloy)$^{-1}$
Temperature gradient in adiabatic zone	G	20 K/mm
Partition coefficient	k	0.029 at%/at%
Slope of liquidus line	m	-2.32 K/at%

distribution of the interface concentration C_I to be obtained.

3.3. Summary of the numerical procedure

The numerical procedure performed at each iteration p of time step k involves the following steps:

- New values for temperature $T^{p,k}$, concentration $C^{p,k}$, vorticity $\zeta^{p,k}$, stream function $\psi^{p,k}$ and velocity vector $\tilde{V}^{p,k}$ are calculated.
- C_I is calculated by extrapolation from $C^{p,k}$ using Eq. (34).
- The melting temperature $T_m^{p,k}$ is found from Eq. (19).
- The liquid fraction $f_l^{p,k}$ at each point of the computational domain is calculated.
- The source term $S_c^{p,k}$ for the solute transport equation and the effective heat capacity coefficient $\partial f_l/\partial T$ are updated.

This procedure is repeated at each iteration until all equations are converged for time step k. Convergence is declared when the average change in the absolute value of each solution variable, relative to the maximum value of that variable, becomes less than a certain tolerance. Typically, the tolerance was in the range 10^{-11}–10^{-8}. The time step is then advanced to $k+1$ and the above procedure is repeated.

[2] In a more recent work we have included conduction in the quartz ampoule as part of the calculation procedure, and have imposed a temperature gradient of 27 K/mm on the outside of the ampoule. This leads to an internal gradient of approximately 20 K/mm, as used here. The isotherms in the sample remain virtually orthogonal to the ampoule axis, although not in the ampoule itself, which has a much lower thermal conductivity.

4. Results and discussion

4.1. Constant melting temperature

The first results presented were obtained with the assumption that T_m does not vary with concentration. Calculations were made for an ampoule 42 mm long and 6 mm across. The magnitude of the gravity vector was taken to be 10 μg, i.e., 9.81×10^{-5} m s^{-2}, acting in a direction normal to the x-axis of the ampoule. The property values of pure liquid bismuth at a reference temperature of 271.3°C (the equilibrium melting temperature) were used (Table 1).

The computational domain initially contained only liquid Bi with a uniform solute concentration C_0 of 1 at% Sn and a uniform temperature of 700°C. The cold end of the ampoule (the left end) had an initial temperature of 272°C. Along the top and bottom boundaries, the temperature increased from the left at 20 K/mm and continued over a length of 21.4 mm until 700°C was reached. From that position onward, the temperature remained constant. The right end of the computational domain had a constant temperature of 700°C. Numerical experimentation showed that the presence of a wall at 42 mm had no effect on the solidification or the flow near the interface for the few mm of solid that were formed. The pulling velocity — the rate of translation of the boundary temperature distribution — was 3.34 μm/s (one of the values used in the MEPHISTO experiment), and was also imposed from $t > 0$. Solidification occurred from left to right as time progressed. The cold end temperature decreased with time in accordance with the imposed temperature gradient until a minimum value of 50°C was reached; thereafter it was kept at 50°C. This temperature distribution was imposed at the liquid boundary, i.e., conduction in the ampoule was not considered.[2]

A uniform square mesh of 210×30 cells (0.2×0.2 mm) was used. Some calculations were also made with

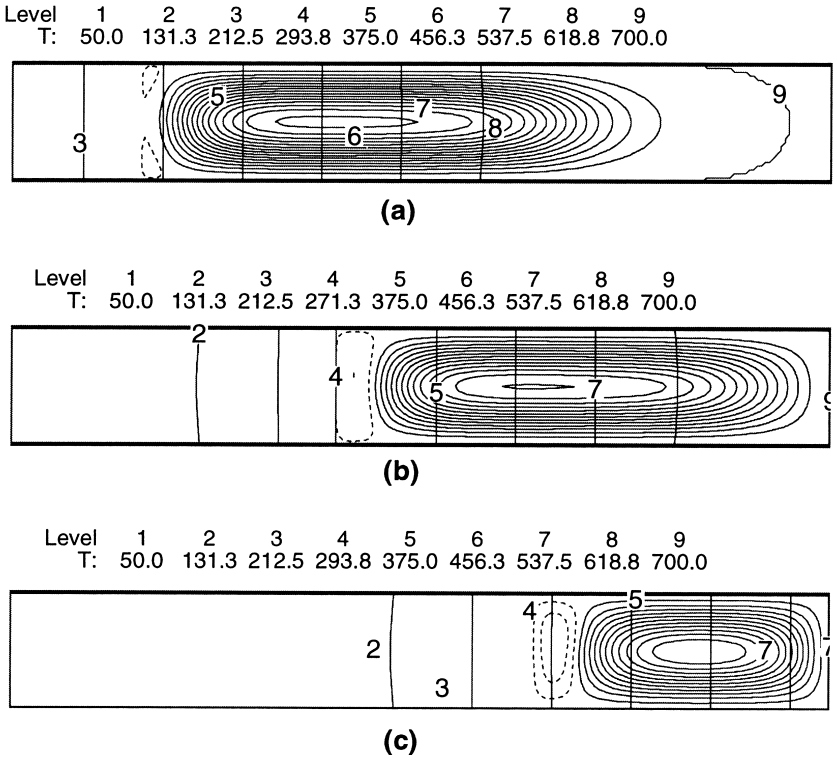

Fig. 2. Stream function contours and isotherms at (a) 2000, (b) 5000 and (c) 8000 s. Dashed lines indicate counter-anticlockwise rotation.

a mesh size of 0.1 mm to ensure that 0.2 mm led to adequate accuracy. After 1000 s of solidification the differences between the two solutions were 1.6% or less for the concentration and velocities.

To validate the numerical solutions obtained using SOLCON, the results were compared [13] with some obtained using the commercial flow code CFX 4.1,[3] which is based on a primitive variable finite volume formulation. Validation of the CFX results was in turn obtained by a comparison of calculations with an experiment in earth gravity using succinonitrile [14]. The agreement between SOLCON and CFX was excellent: within 2.2% for some relevant quantities.

The computations were performed for 8000 s (approximately 27 mm) of solidification. When solidification first starts, the positive temperature gradient in front of the interface leads to a negative density gradient, and the predominant flow direction is downwards (in the direction of $\tilde{g}$). With the gradual build-up of solute in front of the interface, the density gradient reverses; liquid starts to rise in the immediate vicinity of the interface Fig. 2 shows stream function contours in the liquid and isotherms in the entire ampoule after 2000, 5000 and 8000 s. At 2000 s, a very weak positive vertical velocity has appeared near the interface in the top and bottom corners; the flow is predominantly thermally driven and counterclockwise. At 5000 s, solutal convection has become stronger and a reverse cell has formed in front of the interface. After 8000 s, this secondary cell has become competitive in strength to the main thermal flow: the non-dimensional stream function in the core of the solutal cell is 1.08×10^{-4} compared with -5.18×10^{-4} in the thermal cell. As solutal convection increases, it affects the segregation of the solute at the interface. Fig. 3 shows the solute concentration across and along the ampoule at 2000, 5000 and 8000 s. In the early stages of solidification, the thermal flow carries low C solute from the bulk of the liquid to the top of the cavity; as the liquid flows down the interface, C increases. With increasing solute concentration in front of the interface, and the consequent reversal of the density gradient and velocity there, the segregation reduces and, starting at about 5000 s, reverses. At 8000 s, there is a strong segregation in which C at the top of the cavity is 22% greater than that at the bottom.

Fig. 4(a) shows the changes in solute concentration along the interface at 2000, 3000, 5000 and 8000 s. The

[3] Obtained from AEA Technology plc, CFDS, 8.19 Harwell, Didcot, Oxfordshire OX11 0RA, UK.

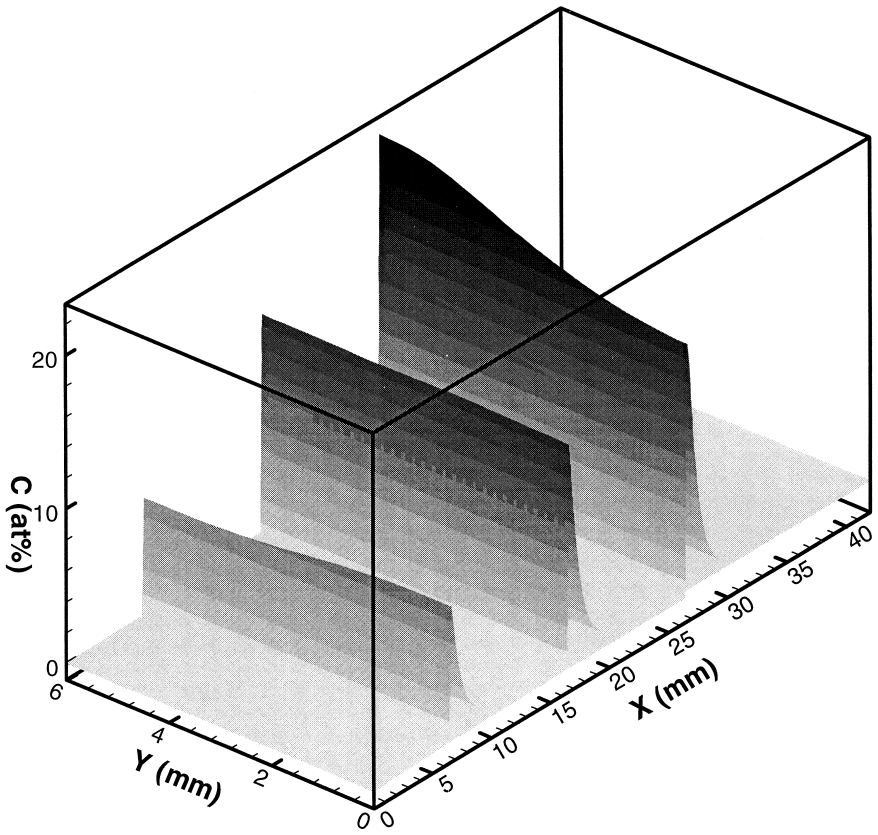

Fig. 3. Solute concentration at 2000, 5000 and 8000 s.

changes in segregation at the interface are shown in Fig. 4(b) (which depicts values computed every 10 s). Due to the convection across the interface induced by the thermal cell, the segregation increased from zero to just over 15% in 2000 s, with the maximum concentration occurring at the bottom of the ampoule. As the solutal cell increased in strength, the balance of convection and diffusion in the solute-rich interface led to a reduction of the segregation, which reached a minimum of about 1% after almost 5000 s. By this time, the solutal-driven reverse flow cell had formed. As it increased in strength, the segregation increased in value again, but now in such a way that the maximum concentration occurred at the top of the ampoule. By 8000 s, it had reached 25%.

Fig. 5 shows contours of solute concentration in the solidified part of the sample after 2000, 5000 and 8000 s of solidification. These contours indicate how a change in the segregation in the liquid affects the distribution of solute in the crystal.

4.2. Concentration-dependent melting temperature

For most materials, the melting temperature T_m is a function of the interface solute concentration C_I. The results presented in this section show the effects of the coupling with the phase diagram on the solidification. The interface solute concentration C_I calculated from Eq. (34) has been used to couple the temperature and solute fields by computing the melting temperature from Eq. (18). Solutions have been obtained for both 1 and 10 μg. Computations have been made for 3000 s of solidification.

The first set of results is for a gravity level of 10 μg. Fig. 6 shows the history of the computed cell average concentration in the liquid portion of the partially solidified control volume (solid lines) and the extrapolated interface concentration (dashed lines). The computed solute concentration oscillates when the front moves from one cell into the next, while the interface solute concentration C_I obtained using extrapolation procedure Eqs. (34)–(36) remains a smooth function. As the volume occupied in a partially solidified cell by the liquid decreases to zero, interface concentration becomes equal to the cell average solute concentration. This explains why the line for the extrapolated concentration passes through the peaks of the zigzags of the line for the cell average concentration.

Fig. 7 shows the position of the moving solid/liquid interface at the mid-height of the ampoule when com-

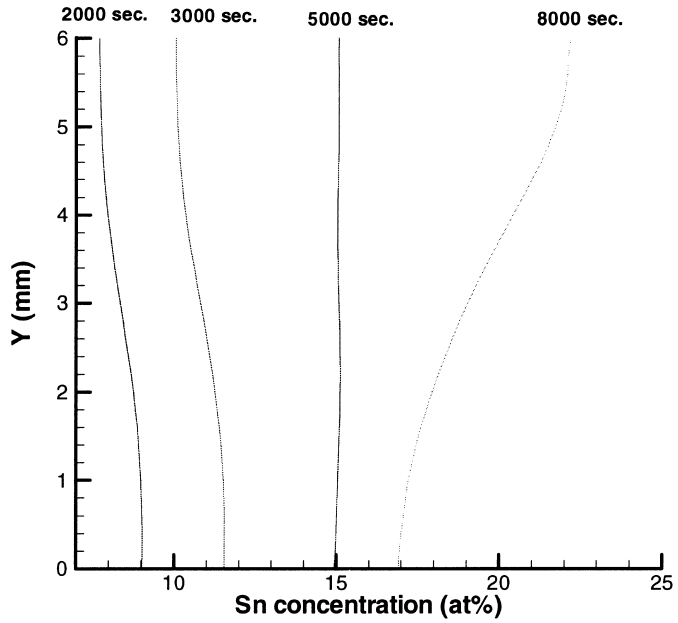

(a)

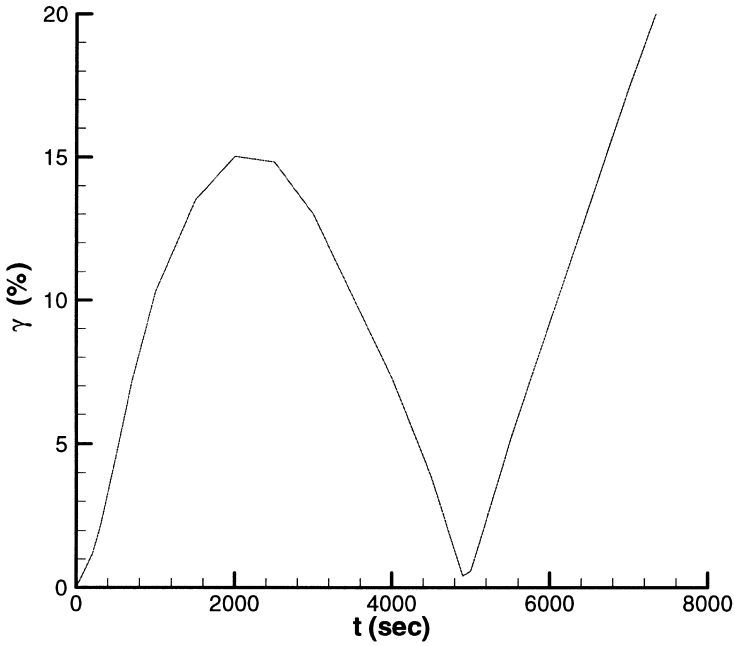

(b)

Fig. 4. (a) Distribution of solute concentration along the interface at 2000, 3000, 5000 and 8000 s. (b) Time history of segregation at the interface.

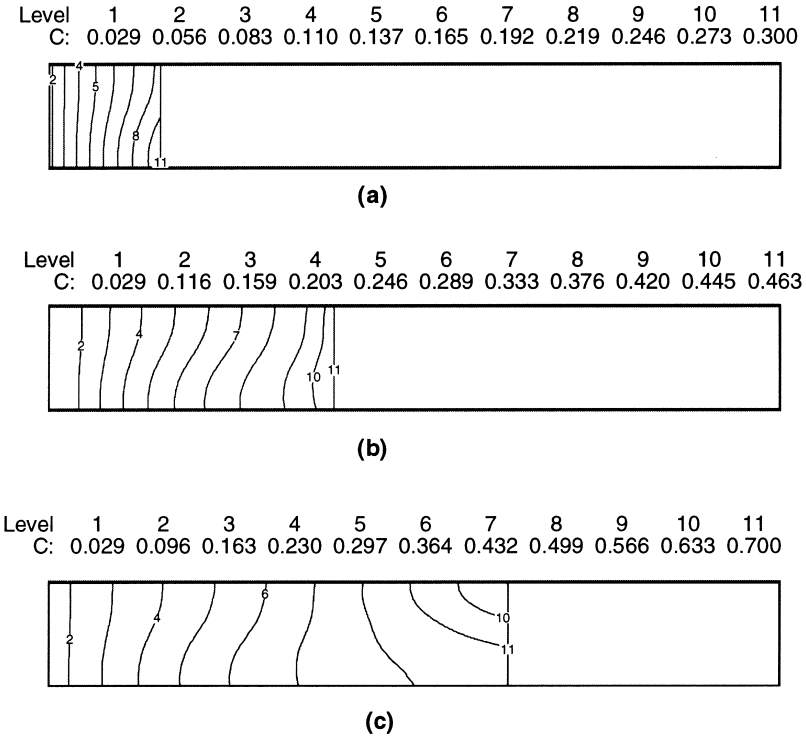

Fig. 5. Contours of solute concentration in the solid part of the sample at (a) 2000, (b) 5000 and (c) 8000 s.

puted using both constant and concentration-dependent melting temperatures. For constant T_m, the interface or growth velocity is the same as the furnace pulling velocity, namely 3.34 μm/s. However, with a concentration-dependent melting temperature, the solute build-up during solidification causes a decrease in the melting temperature and a consequent reduction

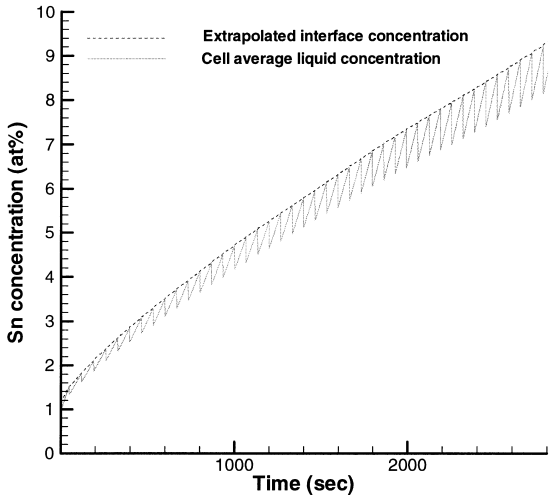

Fig. 6. Time history of the computed average concentration in the liquid portion of the partially solidified cell (solid lines) and extrapolated interface concentration (dashed lines) at the mid-height of the ampoule.

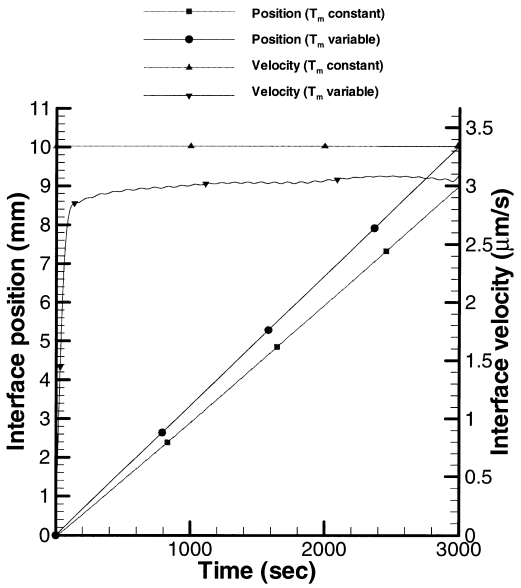

Fig. 7. Position and velocity of the interface at the mid-height of the ampoule computed with constant and with concentration-dependent melting temperature.

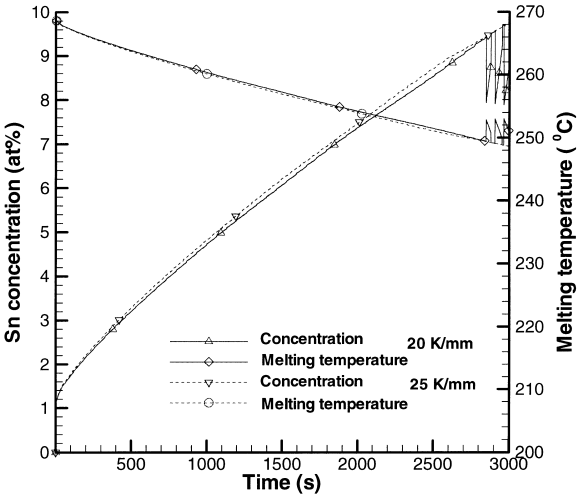

Fig. 8. Time history of solute concentration and melting temperature at the mid-height of the interface with temperature gradient 20 K/mm (solid lines) and 25 K/mm (dashed lines).

in the rate of interface movement (dashed line). This is a transient effect, and if solidification continued until the eutectic composition was reached, the growth and pulling velocities would become the same.

The histories of the interface solute concentration and corresponding values of melting temperature at the mid-height of the interface are shown in Fig. 8. The solid lines are results obtained with a temperature gradient, G, in the transition zone of 20 K/mm. The interface solute concentration C_I rises during solidification from 1 at% to about 10 at% causing a decrease in the melting temperature of about 21°C. After about 2800 s of solidification, the results showed oscillations in C_I, which can be explained by considering the condition necessary for stable plane front solidification. According to the theory of constitutional supercooling (e.g., Flemings [15]), instability of the plane front (leading to a cellular interface) can occur when the liquid immediately in front of the interface has a temperature which is below its equilibrium liquidus temperature (i.e., below its melting temperature). In this condition, the liquid is said to be supercooled. Constitutional supercooling will not occur when the actual temperature gradient in the liquid in front of the interface is equal to or greater than the melting temperature gradient corresponding to the local solute concentration gradient. The melting temperature gradient can be derived from the interface condition Eq. (35) and Eq. (18) for T_m:

$$\left(\frac{\partial T_m}{\partial x}\right)_I = m\left(\frac{\partial C}{\partial x}\right)_I = -\frac{R}{D}m(1-k_p)C_I. \tag{37}$$

Therefore, the front is stable when

$$\left(\frac{\partial T}{\partial x}\right)_I \geq -\frac{R}{D}m(1-k_p)C_I. \tag{38}$$

The maximum value of C_I, which does not exceed the constitutional supercooling criterion, can be estimated from Eq. (38). As noted above, during the initial transient the actual growth velocity is not equal to the pulling velocity. From Fig. 7, the average growth velocity R is 3.04 μm s^{-1}. Recalling that the imposed temperature gradient G is 20 K/mm and noting that $m = -2.32$ K/at%, instability can be expected when the maximum value of the interface solute concentration exceeds 7.99 at%.

Results computed with $G = 25$ K/mm are shown by the dashed lines in Fig. 8. For this temperature gradient, the maximum value of C_I permitted by the constitutional supercooling criterion is 9.99 at%. The concentration had not reached this value at any point on the interface by 3000 s. Thus supercooling was absent and the curves for $C_I(t)$ and $T_m(t)$ corresponding to this gradient remain smooth.

Fig. 9(a) shows the solute concentration distributions at the mid-height of the ampoule at 1000, 2000 and 3000 s for $G = 20$ K/mm. Fig. 9(b) shows the melting temperature distributions (solid lines) resulting from the solute distributions shown in Fig. 9(a) and the actual temperature distributions (dashed lines). Because of the high thermal conductivity of Bi, the temperature field is not significantly affected by convection and the slope of these lines is the same as the imposed gradient of 20 K/mm. At 1000 and 2000 s the peak values of concentration at the interface are less than the limiting value, the actual temperature gradient is above the melting temperature gradient, and therefore supercooling is absent. The melting temperature gradient reaches and then exceeds the actual temperature gradient very close to 3000 s causing an instability of the plane front solidification. The liquid temperature becomes equal to the melting temperature not only at the interface, but also at some small distance away from the interface. As a result, two adjacent control volumes in the direction of solidification undergo phase change at the same time. In practical terms, this means that the interface is no longer sharp and solidification is taking place over a temperature range.

Fig. 10 shows the effect of the magnitude of g on the distribution of solute concentration along the interface (a and b) and position of the interface (c and d) at 1500, 2000, 2500 and 3000 s. Dashed lines in Fig. 10(a) and (b) correspond to the parts of the interface at which instability of the plane front appeared and in front of which supercooled liquid existed. These regions are shown by dots in Fig. 10(c) and (d), which identify the adjacent control volumes in both of which

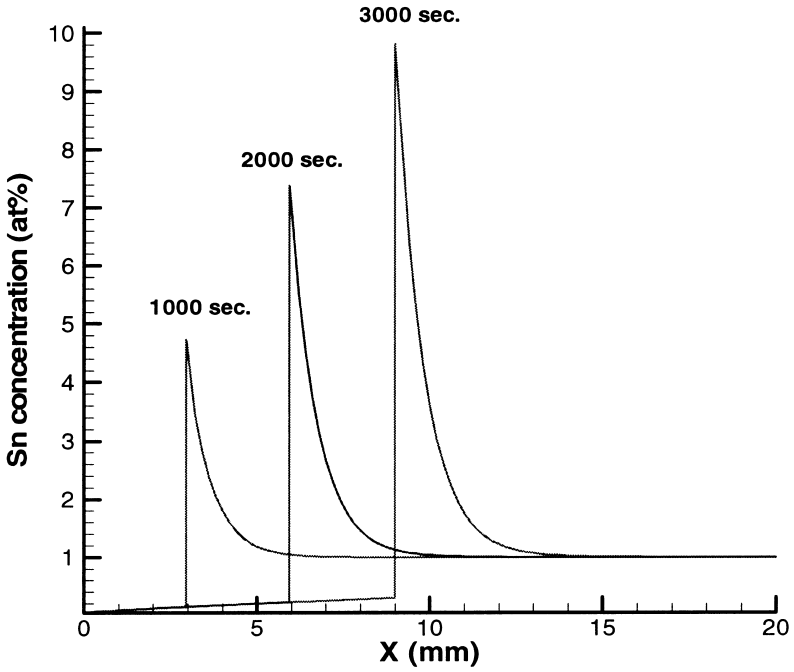

(a)

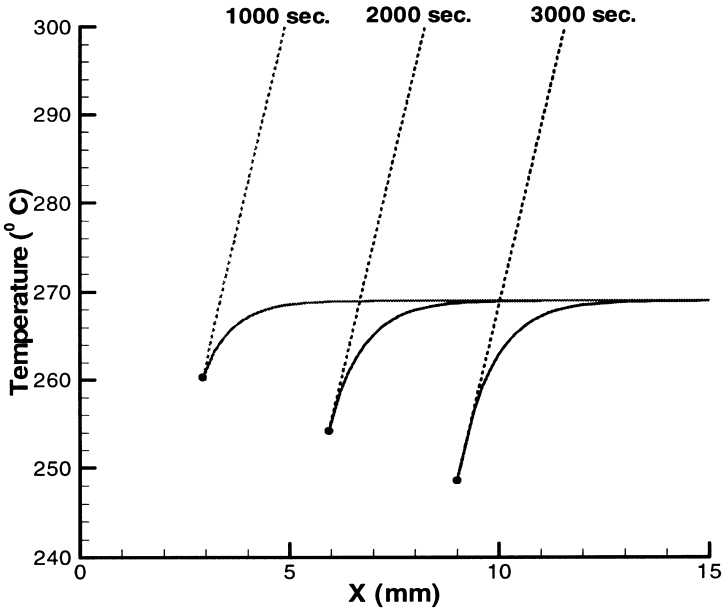

(b)

Fig. 9. (a) Distribution of solute concentration at the mid-height of the ampoule at 1000, 2000 and 3000 s. (b) Distribution of melting temperature (solid lines) and the actual temperature distribution (dashed lined) at the mid-height of the ampoule at 1000, 2000 and 3000 s.

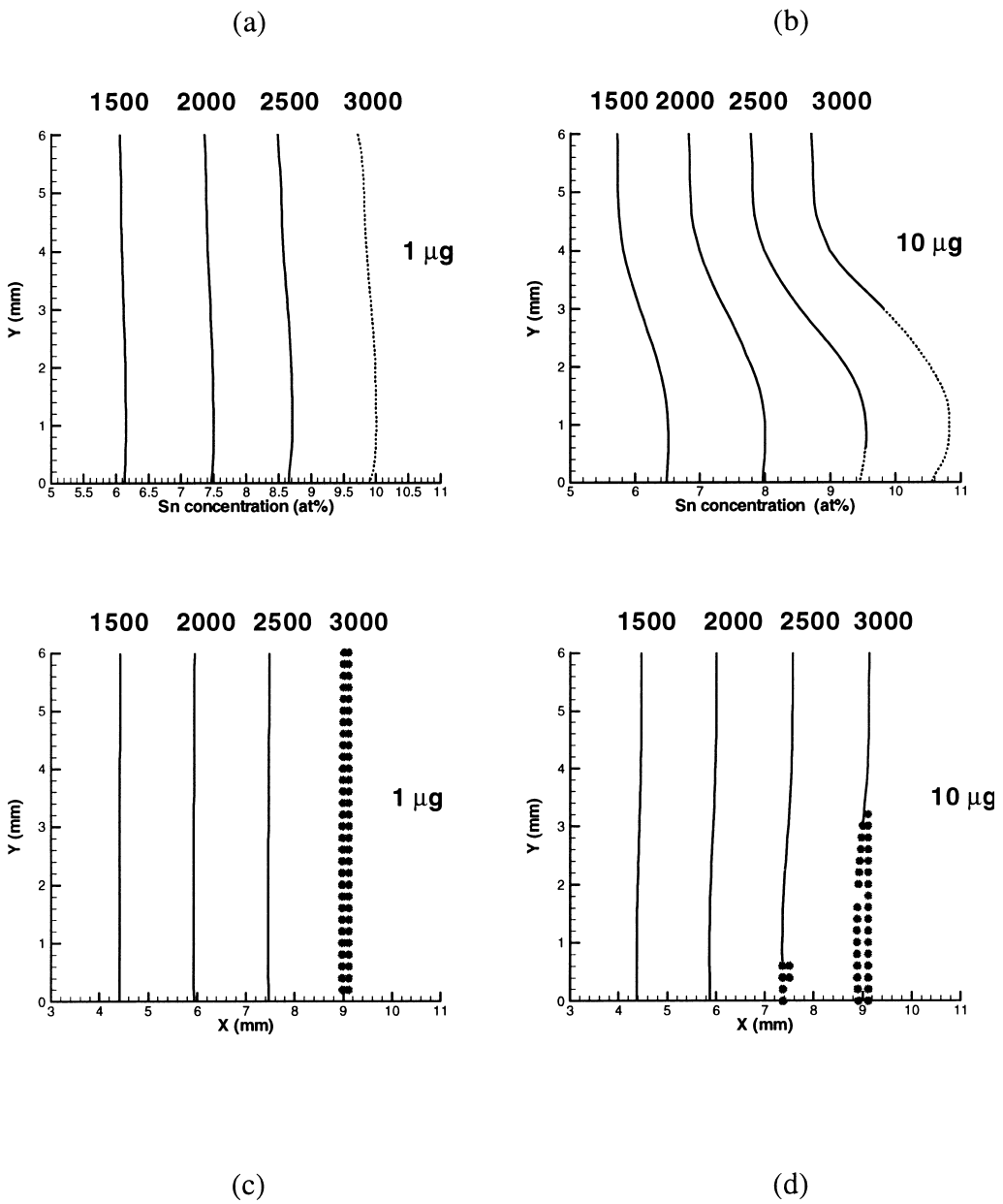

Fig. 10. Distribution of solute concentration across the interface (a and b), and position of the interface (c and d) at 1500, 2000, 2500 and 3000 s for 1 and 10 μg. Dotted lines indicate instability of the plane front.

solidification is occurring. Instability appears earlier at 10 μg due to the higher solute segregation which builds up at the interface. By 2500 s, the segregation of solute at the interface at 10 μg was 20.6% whereas for 1 μg it was 2.65%. The segregation at 10 μg is such that the concentration near the bottom of the cavity exceeds 9.4 at% (Fig. 10(b)) while at 1 μg the concentration remains less than 8.7% as shown in Fig. 10(a). The numerical solutions show instability when the solute concentration exceeds 9.4 at%. On the discrete level, instability appears when the cell adjacent to the partially solidified control volume in the direction of increasing x becomes supercooled, i.e. the cell boundary temperature becomes less than T_m and hence the liquid fraction in this control volume lies between 0 and 1. Therefore the constitutional supercooling criterion has to be applied at this cell boundary. If we consider $C_{cr} = 7.99$ at% as the limiting cell boundary

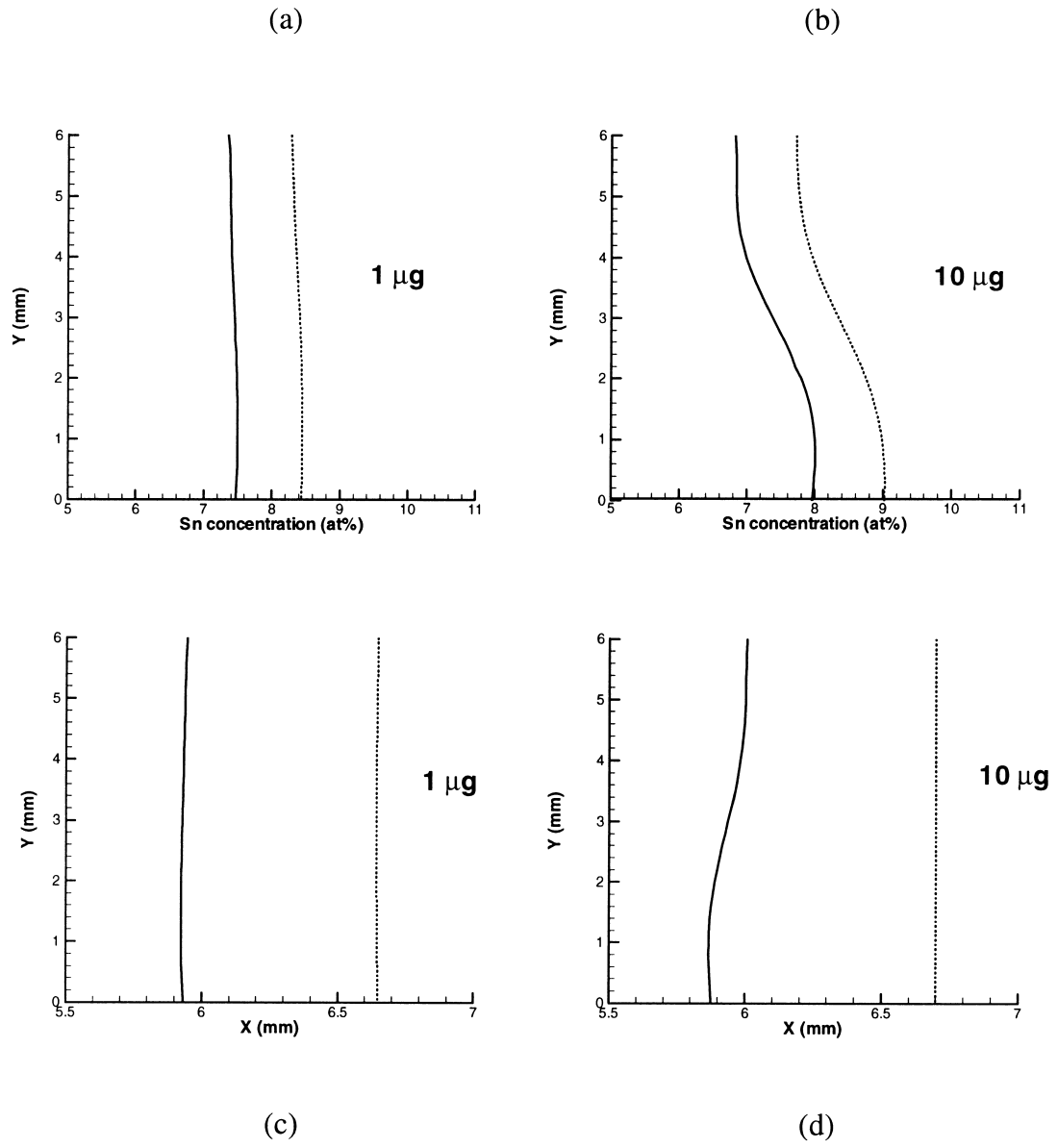

Fig. 11. Distribution of solute concentration along the interface (a and b), and position of the interface (c and d) after 2000 s of solidification for constant (dashed lines) and concentration-dependent (solid lines) melting temperature for 1 and 10 μg.

value the limiting value for interface concentration can be found by applying Eq. (34) at $\xi = f_l \Delta x$ and using a truncated Taylor series. This yields to

$$(C_I)_{cr} = C_{cr}\left(1 + \frac{R}{D}(1 - k_p) f_l \Delta x\right) \tag{39}$$

It is clear that $(C_I)_{cr}$ depends on the actual position of the interface within the partially solidified control volume, which is determined by the cell liquid fraction. For a partially solidified cell in front of which supercooled liquid exists, as shown in Fig. 10(b) for 2500 s, $f_l = 0.7062$ and the estimated critical concentration is $(C_I)_{cr} = 9.21$ at%.

Values of solute concentration at the interface and the position and shape of the interface after 2000 s of solidification are shown in Fig. 11 for two values of g and for constant (dashed lines) and concentration-dependent (solid lines) melting temperature. Inclusion of a concentration-dependent melting temperature in the computations has only a small effect on segregation at the interface, changing it from 17.05% for constant

T_m to 16.05% for variable T_m at 10 μg, and from 1.99 to 1.97% at 1 μg, respectively. Segregation is more strongly affected by gravity level. Values of concentration at the interface are smaller in the case of $T_m(C)$ due to the shorter distance of solidification as indicated in Fig. 11(c) and (d).

If T_m is constant, the interface is represented by an isotherm and remains virtually flat (i.e. parallel to the y-axis). However, when T_m is concentration-dependent, segregation (especially at 10 μg) causes the interface to be curved, and it is no longer an isotherm. Differences in the shape of the solid/liquid interface determined by differences in the segregation at 1 and 10 μg can be seen in Fig. 11(c) and (d). The flow patterns in the two cases (not shown) are very similar.

5. Conclusion

A method for the computational study of directional solidification based on the fixed grid single domain approach has been described. The enthalpy method is used to solve for the temperature field over the computational domain including both the solid and liquid phases and to estimate the location of the solid/liquid interface. A source term accounting for the release of solute into the liquid during solidification has been incorporated into the solute transport equation. The vorticity–stream function formulation is used to describe thermosolutal convection in the liquid region.

The liquid fraction in a partially solidified cell is used to describe concentration changes within one control volume due to solidification. In some ways this is analogous to explicit interface tracking with information about the liquid fraction being used to estimate the interface location at each time step.

A fixed grid single domain approach, when implemented to solve for the solute concentration using the source term derived by Voller [7], gives solutions, which are averaged over the computational cells. To find the concentration at the interface, an extrapolation procedure is needed to recover the interfacial values from the computed cell average values. We have shown that the proposed extrapolation procedure leads to a distribution of interface concentration over time which is smooth and which satisfies the computed values at those times when the interface passes through a cell boundary. Knowing the actual interface concentration is essential if coupling with the phase diagram (a concentration-dependent melting temperature) is to be included in a solidification model. Under microgravity conditions, the flow produced by both the thermal and the solutal concentration gradients is very weak. However, the effect of this weak flow on segregation cannot be dismissed, even at 1 μg. If convection is neglected and only diffusion is considered, no segregation will be produced. The numerical results show that this is definitely not the case.

The results also show clearly that it is important to include the effect of solute concentration on the melting temperature in a solidification simulation. The velocity of the interface is determined not just by the pulling speed but also by the rate at which the interface concentration is increasing.

Acknowledgements

The UNSW authors acknowledge with thanks the support of the Australian Research Council and the Australian Department of Industry, Science and Technology. They also express their gratitude to H.C. de Groh III, NASA Lewis Research Center, for the opportunity to participate in MEPHISTO-4 and his continual collaboration during this research.

References

[1] C.J. Chang, R.A. Brown, Radial segregation induced by natural convection and melt/solid interface shape in vertical Bridgman growth, J. Crystal Growth 63 (1983) 343–364.
[2] P.M. Adornato, R.A. Brown, Convection and segregation in directional solidification of dilute and non-dilute binary alloys: effects of ampoule and furnace design, J. Crystal Growth 80 (1987) 155–190.
[3] J.I.D. Alexander, J. Ouazzani, F. Rosenberger, Analysis of the low gravity tolerance of Bridgman–Stockbarger crystal growth: I. steady and impulse accelerations, J. Crystal Growth 97 (1989) 285–302.
[4] M. Yao, R. Raman, H.C. de Groh III, Numerical simulation of heat and mass transport during space crystal growth with MEPHISTO. NASA Technical Memorandum 107015, 1995.
[5] W. Bennon, F. Incropera, A continuum model for momentum, heat and species transport in binary solid–liquid phase change systems: I. Model formulation, Int. J. Heat Mass Transfer 30 (1987) 2161–2170.
[6] W. Bennon, F. Incropera, A continuum model for momentum, heat and species transport in binary solid–liquid phase change systems: II. Application to solidification in a rectangular cavity, Int. J. Heat Mass Transfer 30 (1987) 2171–2187.
[7] V.R. Voller, A.D. Brent, C. Prakash, The modelling of heat, mass and solute transport in solidification systems, Int. J. Heat Mass Transfer 32 (1989) 1719–1731.
[8] X. Zeng, A. Faghri, Temperature-transforming model for binary solid–liquid phase-change problems: I. Mathematical modelling and numerical methodology, Numerical Heat Transfer 25B (1994) 467–481.
[9] K. Morgan, R.W. Lewis, O.C. Zienkiewicz, An improved algorithm for heat conduction problems with phase change, Int. J. Numer. Meth. Eng 12 (1978) 1191–1195.

[10] A.A. Samarskii, V.B. Andreyev, On a high-accuracy difference scheme for an elliptic equation with several space variables, USSR Comput. Math. and Math. Phys 3 (1963) 1373–1382.
[11] P. Tamamidis, D.N. Assanis, Evaluation of various high-order accuracy schemes with and without flux limiters, Int. J. Num. Methods in Fluids 16 (1993) 931–948.
[12] V.G. Smith, W.A. Tiller, J.W. Rutter, A mathematical analysis of solute redistribution during solidification, Canadian J. Physics 33 (1955) 723–743.
[13] V. Timchenko, P.Y.P. Chen, G. de Vahl Davis, E. Leonardi, H.C. de Groh III, in: J.S. Lee (Ed.), Directional Solidification in Microgravity: Heat Transfer 98, Taylor & Francis, London, 1998, pp. 241–246.
[14] P.Y.P. Chen, V. Timchenko, E. Leonardi, G. de Vahl Davis, H.C. de Groh III, A Numerical study of directional solidification and melting in microgravity, in: HTD-Vol. 361-3/PID-Vol. 3, Proc. ASME Heat Transfer Division, 1998, pp. 75–83.
[15] M.C. Flemings, Solidification Processing, McGraw-Hill, New York, 1974, pp. 58–61.